Development of a robot-based test bench for the destructive testing of components

Julia Reichmann, Julian Hanke, Christian Eymüller, Anna Trauth, Wolfgang Reif, Markus G. R. Sause

Angaben zur Veröffentlichung / Publication details:

Reichmann, Julia, Julian Hanke, Christian Eymüller, Anna Trauth, Wolfgang Reif, and Markus G. R. Sause. 2025. "Development of a robot-based test bench for the destructive testing of components." Journal of Testing and Evaluation 53 (1): 42–58. https://doi.org/10.1520/jte20240091.

Journal of Testing and Evaluation

doi:10.1520/JTE20240091 / Vol. 53 / No. 1 / 2025 / available online at go.astm.org/pubs

Julia Reichmann,[1] Julian Hanke,[2] Christian Eymüller,[2] Anna Trauth,[3] Wolfgang Reif,[2] and Markus G. R. Sause[3]

Development of a Robot-Based Test Bench for the Destructive Testing of Components

Reference

J. Reichmann, J. Hanke, C. Eymüller, A. Trauth, W. Reif, and M. G. R. Sause, "Development of a Robot-Based Test Bench for the Destructive Testing of Components," *Journal of Testing and Evaluation* 53, no. 1 (January/February 2025): 42–58. https://doi.org/10.1520/JTE20240091

ABSTRACT

This paper presents a novel approach for robot-based mechanical testing on the component level using a high degree of flexibility in the superimposition of loads, which allows their application to test various geometries and conditions. To validate our approach, tensile tests were performed using different control modes: position control, force control using a six-axis force/torque sensor, and path control using optical tracking of markers. The last two sensor-guided control modes are used to compensate unwanted force components that may occur in a system with six degrees of freedom. For reference, the same tests were performed on a conventional universal testing machine and were in good agreement. Subsequently, the flexibility of the robot-based test setup is demonstrated by two different component tests; a bicycle frame and a snowboard with high compliance were examined with different load cases. It was demonstrated that in path control mode an improvement in the accuracy of absolute positioning occurs and compensation for any transverse forces is possible. In addition, the path control mode enables the preservation of the initial load vector relative to the surface, even under significant deformation of the component.

Keywords

component testing, robot-based testing, mechanical testing, force control, path control, robotics

Manuscript received February 9, 2024; accepted for publication November 1, 2024; published online December 19, 2024. Issue published January 1, 2025.

[1] Institute of Materials Resource Management, University of Augsburg, Am Technologiezentrum 8, Augsburg 86159, Germany (Corresponding author), e-mail: julia.reichmann@mrm.uni-augsburg.de, https://orcid.org/0009-0000-2495-0690

[2] Institute for Software & Systems Engineering, University of Augsburg, Universitätsstraße 6a, Augsburg, 86159, Germany

[3] Institute of Materials Resource Management, University of Augsburg, Am Technologiezentrum 8, Augsburg 86159, Germany

Introduction

The mechanical robot-based component testing approach is a fundamentally new concept and an emerging field of research. It offers new degrees of freedom to apply loads on

components and improved flexibility to perform different tests due to the high flexibility of six-axis robotic systems.

In contrast to robot-assisted methods, in which robots only support the testing procedure by inserting the specimen, in robot-based methods, the industrial robots perform the entire testing process. Robot-assisted methods are already widely implemented in medical technology, e.g., to analyze dental adhesive materials' stability and thermal aging.[1] The thermocycling process is performed by an industrial robot that cyclically immerses the sample basket (with the teeth to be tested) in different temperature environments.[1]

In (industrial) manufacturing, both approaches, either robot-based or robot-assisted, play a significant role in automation and process control. They are used, for instance, to improve the surface quality during the milling process by compensating for the cutting forces that occur (robot-based),[2] as well as checking the tolerance and quality of resistance spot welds (robot-assisted).[3] Another application of robot-assisted or robot-based testing is the field of nondestructive testing. Fully autonomous, nondestructive ultrasonic testing of complex curved workpieces is possible using a robot-assisted trajectory planning method.[4] Challenging tasks such as 3-D scene reconstruction, target recognition, and path planning can be successfully mastered with computer vision and robotics. This increases the flexibility, reliability, and adaptability of robots compared with conventional manual approaches.[5]

Within the framework of robot-based nondestructive testing, Mineo and Javadi[6] summarize further approaches for in-process inspections in manufacturing applications (robotic wire-arc welding and additive manufacturing), real-time and data-driven robot-enabled sensing, and mobile robotic platforms.

Approaches for the robot-assisted mechanical testing of components are also commercially available. One example is the roboTest R automated testing system from ZwickRoell GmbH & Co. KG. Specimen mounting and unmounting, testing, and removal of the specimen residues are fully automated by industrial robots. However, the roboTest R is only designed for the classic tests such as tensile, compression, bending, and notched bar impact tests and for the typical standardized test specimens. This test setup is not intended for more complex components.

In general, the disadvantage of robot-assisted mechanical testing is the necessity of additional equipment such as a universal testing machine or a testbed. For example, the handling of specimens does not exploit the potential of the industrial robot unless it is a key task that happens repetitively and therefore results in higher turnover of samples. To optimize the economical footprint of robots in mechanical testing, more flexibility should be achieved both in the load application and in the shape and size of the test specimens or components.

For reasonably complex load cases, specific test stands have been established. One system (OccuBot) has been developed by KUKA AG, which uses industrial robots for robot-based testing of vehicle and aircraft seats. The test system investigated by Beeh and Wörn uses OccuBots for seat testing and compensates the static forces caused by the weight of the test dummy.[7] An alternative approach for robot-based destructive testing was proposed using a Stewart platform (Hexapod) instead of a six-axis industrial robot. For example, the Technical University of Hamburg-Harburg is researching the dynamic testing of aircraft galleys under realistic conditions. Another application for the Stewart platform as a testing machine is a tension-shear test on a notched concrete specimen (Nooru-Mohamed experiment).[8] The simulation of realistic load cases also plays an essential role in medical technology. Robot-based testing is considered to simulate human movements, such as chewing,[9] by using a Stewart platform or by simulating movements of the knee joint[10] with an industrial robot. However, all the mentioned applications are designed for one specific load case and a specific test specimen type.

To realize a fully flexible robot-based mechanical testing approach, this paper presents a new concept for a configuration that includes a test setup adjustable to the application with two six-axis industrial robots and appropriate instrumentation. The industrial robots not only allow the execution of standard load cases—namely tension, compression, and torsion—in any spatial direction, but also enables the superposition of different load cases. In addition, the described approach allows the testing of various components, with the additional possibility of collaborating industrial robots.

The flexibility of this approach enables highly specialized component testing and extends to handling a wider range of test scenarios. As a result, component testing has evolved from a specialized to a universal concept.

Materials and Methods

ROBOT-BASED TESTING SETUP

The setup of the robot-based test bench with focus on the underlying control system has already been described.[11] The most important components of the system are briefly summarized in the following and are extended in the context of mechanical testing. An overview of the system is depicted in **figure 1**.

The load for the component testing is applied by two KR1000 Titan six-axis industrial robots from KUKA AG, each with a payload of 1,000 kg (see #1 in **fig. 1**). The reachability and capacity allow high flexibility in terms of component size, placement, load application, and variability of the load paths. In addition, both robots are equipped with a six-axis force/torque sensor (type: K6D175 from ME-Messsysteme, measurement range 50 kN/5 kNm, accuracy class 0.2 %) (see #4 in **fig. 1**), and a measuring amplifier (type: GSV-8DS EC/SubD44H from ME-Messsysteme). The robots are arranged opposite to each other around a clamping field (7 m × 2.5 m) (see #2 in **fig. 1**). In addition, traditional mounting fixtures, e.g., a clamping angles (see #3 in **fig. 1**), are used to fix specimens and components on the clamping field. An optical metrology system (type: ATOS 5, Carl Zeiss GOM Metrology GmbH) is used to perform optical tracking of markers as a 3-D-extensometer and is able to operate as a digital image correlation (DIC) system to perform 3-D full field strain measurements (see #5 in **fig. 1**).

TESTING SEQUENCE

A typical test sequence of robot-based component testing consists of an approach motion, a testing motion, and a departure motion. **Figure 2**, which is based on work by Hanke et al.,[11] shows a schematic test sequence for robot-based component testing. The approach motion can either be position- or contact-based. Preloads or positions are applied in this step. This can be a precondition for terminating the approach motion. The subsequent testing motion is generated with the help of a sensor-guided position correction via the robot sensor interface (RSI). This technology package developed by KUKA AG serves as a universal interface for KUKA robots and enables the fine-tuning of predefined robot motions with live sensor data. The test motion can be divided into sensor-guided motions (path or force control) and position-controlled motions solely based on the robot kinematics calculation. The sensor-guided motions are based on the data provided by either the force/torque sensors or the optical measurement system. It is a control loop comparing a target value with a current value. Hence, occurring

FIG. 1

Setup of robot-based component testing with two six-axis industrial robots, a clamping field, and clamping angle for flexible positioning and clamping of test specimens and components.

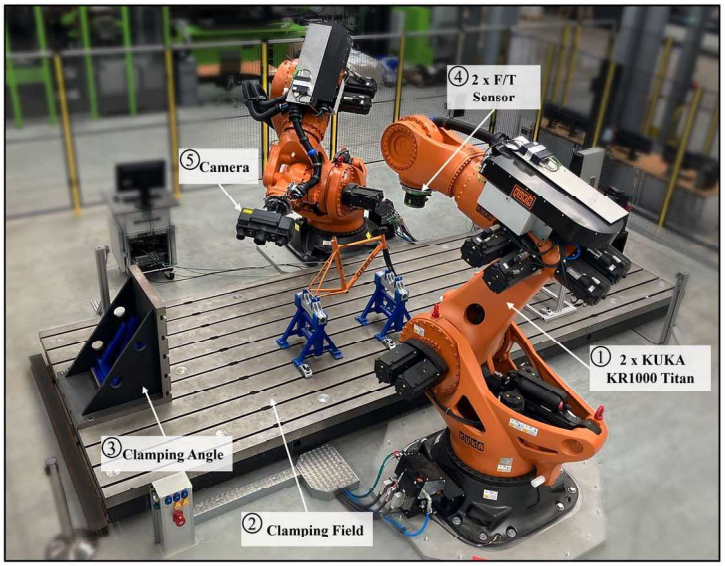

FIG. 2 Test sequence of a robot-based component test with the associated test parameters and requirements.

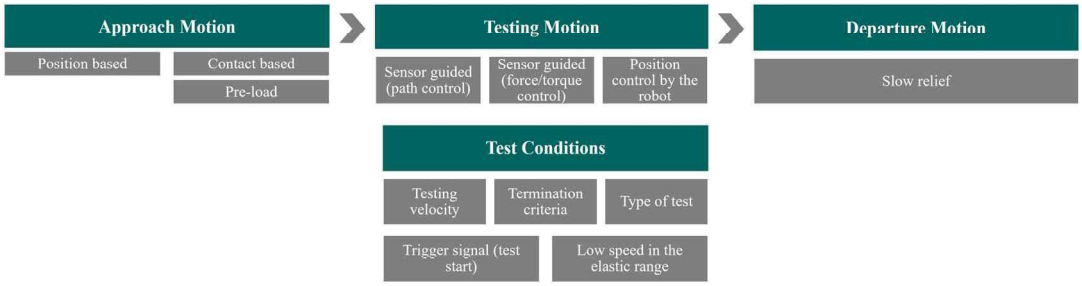

deviations are corrected in real-time by adapting the robot movement. This correction has no influence on the testing velocity. In addition to the type of motion, test conditions can be specified. These include typical mechanical test settings such as the type of test (tension, compression, bending, torsion, or a superimposed load), the testing velocity (displacement per time), and the termination criteria for the test motion, but also other boundary conditions such as a trigger signal for the start of the test and the option of moving through the elastic range more slowly using appropriate control conditions. The termination criteria for the testing motion is set to end when the load is reduced to 20 % of the maximum load. The final phase of the test is the departure motion, during which the robot exits the testing area. This ensures a safe and controlled unloading of the specimen or component.

DATA FLOW AND PROCESSING

Figure 3, according to Hanke,[12] schematically shows all sensor systems and actuator data flow and their further processing. The force is controlled via the force/torque sensor attached to the industrial robot, which has a measuring frequency 250 Hz and provides its data with an EtherCAT interface. The sensor data, in this case, three force (F_x, F_y, F_z) and three torque values (T_x, T_y, T_z), are sent to the data aggregation of the central control unit. Similarly, path control works via the optical measurement system. In this case, relative displacements (D_x, D_y, D_z) and rotation angles (D_α, D_β, D_γ) between the test fixture on the industrial robot end effector and the component are sent to the data aggregation via Standard Commands for Programmable Instruments (SCPI) interface with the maximum system frequency of 10 Hz. At the same time, position data are sent from all robots to the data aggregation every 4 ms (equivalent to 250 Hz) via RSI. The position data required to clearly define the pose of an industrial robot are as follows: the coordinates (X, Y, Z), the orientation (A, B, C), as well as

FIG. 3 Overview of the data flow and processing of robot-based component testing.

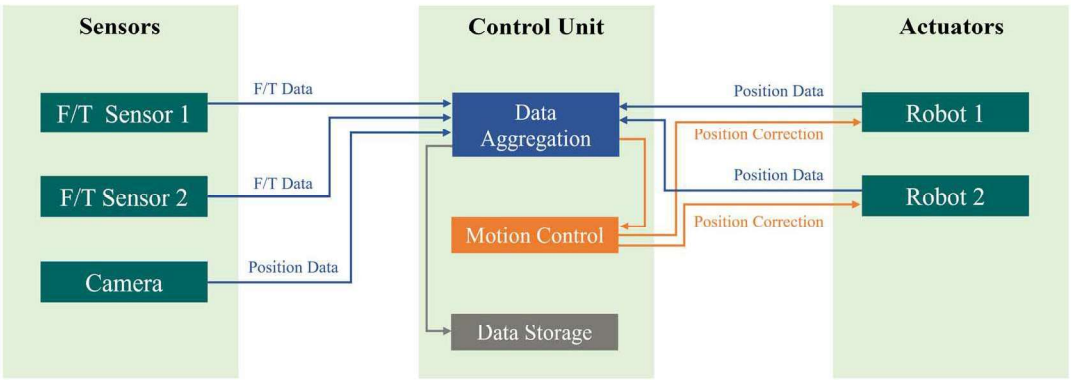

status (*S*), and turn (*T*). Status and turn define a unique axis position from several possible axis positions for the same position (KUKA specific). The data of the aforementioned acquisition systems are recorded with different frequencies. Consequently, a synchronized time stamp is sent with the data and adjusted to a common frequency of 250 Hz by linearly extrapolating data points, if necessary. Subsequently, the data are turned into a subsequent vector containing information on loading direction and testing velocity and are passed to the motion control to execute a specific motion of the robots. Because of the continuous sensor data acquisition, the motion can be readjusted precisely according to the desired criteria every 4 ms. As already described in Hanke et al.[11,13] because of the compliance of the industrial robot kinematics, it is challenging to predict a strictly linear motion in a distinct direction without adjusting the motion with the help of the corresponding sensors. This is especially relevant when the industrial robot is additionally subject to external load, which is not anticipated by the underlying internal kinematics model of the robots. With the help of the sensor-guided test motion, this can be realized and compensated. In addition, this allows for actively compensating the transverse forces or displacements in undesired directions. Finally, the recorded data is stored in the data storage to be further used for offline evaluation.

TEST SETUPS

The different test scenarios performed to validate the test setup are described in detail in the following. First, uniaxial tensile testing was used to generate a pure uniaxial stress state without transversal forces. Standardized tensile testing based on a universal testing machine served as a reference for validating the accuracy, the test motions, and the material properties. Subsequently, more complex load cases were realized by loading representative components, such as a bicycle frame and a snowboard. With the bicycle frame, a sequence of different load cases introducing forces at different positions of the components was realized. For the snowboard, the focus was on load cases with superimposed forces (bending and torsion loads) and the ability to update the initial load vector in situations of high system compliance.

The coordinate systems for the respective sensors and actuators were adapted to each new test setup. In general, the industrial robot and camera coordinate system are based on the internal coordinate system of the force/torque sensor because this cannot be adjusted. This ensures that all forces, torques, displacements, and rotations of the various sensors and actuators match each other. The respective coordinate system for the discussion of the results is included in the respective test setup illustrations.

Uniaxial Stress States Without Transverse Forces

This stage of the validation serves as a proof of concept to verify the robot-based component testing and motion control systems that were mentioned before. As previously described in Hanke et al.[11,13] the whole setup has to deal with the following challenges:

- Industrial robots are typically not designed for slow velocities required for material testing.
- The industrial robot dynamic model lacks absolute positioning when the system is additionally subject to external loads.
- Transverse forces or superimposed torque may occur during the test resulting from deviations of the intended test motion.

To overcome these challenges, the test movements were adapted using sensor guidance. In this study, three different motion controls were performed: force-controlled, path-controlled, and position-controlled via the internal robot kinematics without additional sensors (see **fig. 2**). The optical measurement system allows for measuring the material elongation as extensometer, as well as by tracking the exact position of the clamping jaws to assess system compliance and possible superimposed rigid body motions.

To validate the robot-based testing (see **fig. 4*A***), reference tests were performed on a universal testing machine (Zwick/Roell Zmart. Pro Z1464, loading capacity: 50 kN, accuracy class 0.5 %) in a laboratory (see **fig. 4*B***) with the same materials and specimen geometries, namely stainless steel (X5CrNi18-10). The three different

FIG. 4 Two different test setups for the tensile test: (*A*) robot-based tensile testing and (*B*) classic setup with a universal testing machine.

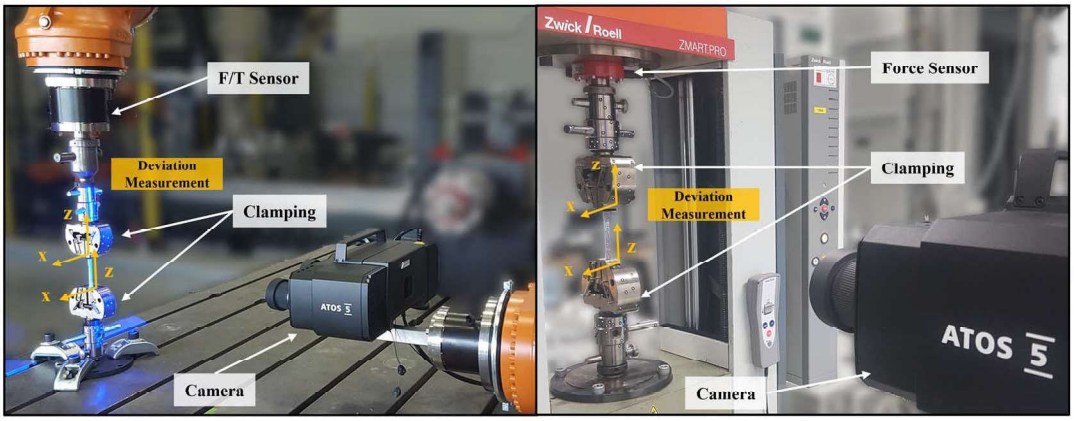

(*A*) (*B*)

control modes of the robot-based testing were each averaged over three specimens, whereas tensile testing in the laboratory was averaged over four specimens. Dog-bone shaped specimens were prepared by water jet cutting with dimensions of 190 mm × 10 mm × 3 mm (overall length × minimum width × thickness). The length of the reduced parallel section is 80 mm. Referring to the material supplier's data sheet, the Young's modulus is 200 GPa and the testing velocity is set to 5 mm/min until a force of 6,000 N is reached, then increased to 10 mm/min until the specimen fails. The same testing procedure and dog-bone termination criteria to stop the test (load drop of 80 % of F_{max}) have been applied for robot-based and conventional testing, respectively. To ensure that the industrial robot achieves the required forces, the specimen placement tool[14] was used. Both test benches used the same optical measurement system ATOS 5 with CP40/MV700 lenses, which can examine a volume of 700 × 530 × 520 mm^3 (calibration deviation: 0.117 pixels). A stochastic pattern was applied to each tensile specimen tested to determine displacements and resulting strain fields in the specimen using DIC. In addition, reference point markers were applied to the clamping jaws to record their movement during the test. Because of the testing setup and requirements from measurement techniques, compromises had to be made in the choice of lens size and resolution. The area of the tensile specimen (gage length × minimum width) is small compared with the total recorded measurement volume, which includes the clamping jaws (pixel size: 0.18 mm/pixels). The incision deviation was checked for all measurements before the respective test was started and is less than 0.1. However, when comparing classic tensile tests on a universal testing machine with robot-based tests, it is important to also track the clamping jaws, test fixture, or the robot end effector to draw conclusions about the quality of motion and control. Therefore, a compromise between the DIC resolution, the region of interest and the available lens systems was required. For a real component test, the optical metrology system running in DIC mode should conform with the recommendations of the International Digital Image Correlation Society (iDICs) to obtain reliable data.[15] This allowed for tracking the movement of the full system, including the crosshead or the industrial robot and test fixture. The tensile specimens tested with the robots were divided into three sets and were tested under force, path, and robot position control. The reference tests with the testing machine were tested under position control. In addition to the comparison of robot-based testing and conventional testing with a universal testing machine in the laboratory, it was also possible to evaluate the effect of the three different robot testing motions.

Variation of Load Vector Position

To investigate the flexibility of the robot-based testing approach, a bicycle frame was chosen for additional evaluation. The frame is made of aluminum alloy and carbon fiber-reinforced plastic (rigid fork). A specialized

FIG. 5

Test setup for bicycle frame testing with three different load cases, shown by arrows.

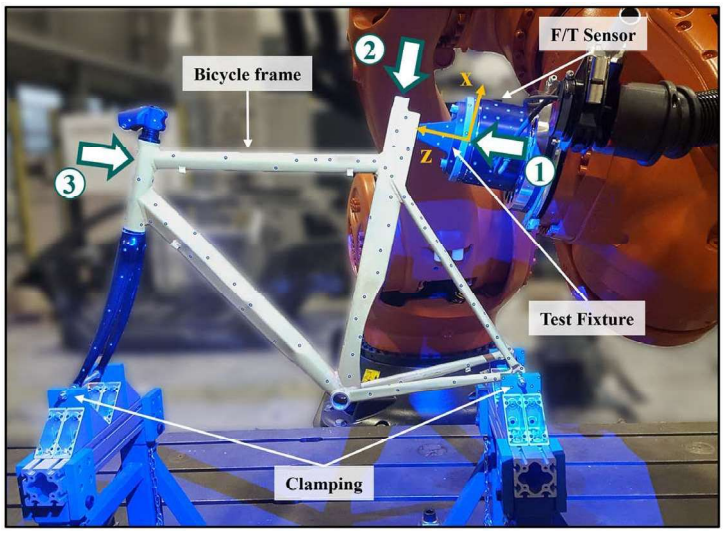

clamping device was designed and attached to the clamping field. In addition, form-closure test fixtures (adapted to the bicycle frame geometry) were designed based on a 3-D scan of the bicycle frame for each respective load case and additively manufactured with a fused deposition modeling process with a carbon fiber reinforced nylon filament (see fig. 5).

Three load cases (marked with numbered arrows in fig. 5) are chosen. The test speed for each load case is 5 mm/min until the compressive force (F_z) reaches 100 N (preload), after which the test continues at 2 mm/min. Load case #1 represents a lateral compressive load up to 500 N on the seat tube; load case #2 represents a compressive load up to 2,000 N on the seat post; and load case #3 represents a lateral compressive load up to 1,000 N on the head tube. All load cases are realized path- and force-controlled. The resulting displacements have been measured by optical tracking of the markers on the bicycle frame. The ATOS 5 was used as optical measurement system with CP40/MV1000 lenses, which can examine a volume of $1{,}000 \times 750 \times 750$ mm^3 (calibration deviation: 0.027 pixels).

Superposition of Load Cases

In the following experiment, a snowboard was considered for testing. This featured significantly higher compliance than the previous specimens and components. In addition, superimposed loads such as bending and torsion are realistic load cases for this component. The snowboard is firmly clamped on the binding on one side. On the other side, which is free to move, load was applied with an additively manufactured test fixture made of glass-fiber–reinforced polymer (see fig. 6). Two different load cases were realized: load case #1 represents a pure bending load because a constant load in the z-direction (orthogonal on the surface) with a constant testing velocity of 50 mm/min was introduced. The global load direction of the force vector was continuously adapted so that the force was always applied perpendicular to the snowboard surface. The resulting trajectory generates a bending of the snowboard. Both path and torque control testing were considered in this experiment. The two types of control differ slightly in their practicability: in the case of torque control, the robot and snowboard must be firmly connected to each other to ensure that controllable transverse forces or torques occur. On the other hand, path control does not require a fixed connection. This approach makes it easier to observe the displacement of the snowboard and, thus, makes the functionality of the load vector adaption and superimposed loads more visible. Load case #2 represents a superimposed bending (F_z) and torsion load (T_y). The testing velocity was set to 50 mm/min in the z-direction, as well as 50 degrees/min and 10 degrees/min for the rotation around

FIG. 6

Test setup for snowboard testing with two different load cases: #1 represents a pure bending load and #2 represents a superimposed bending and torsion load.

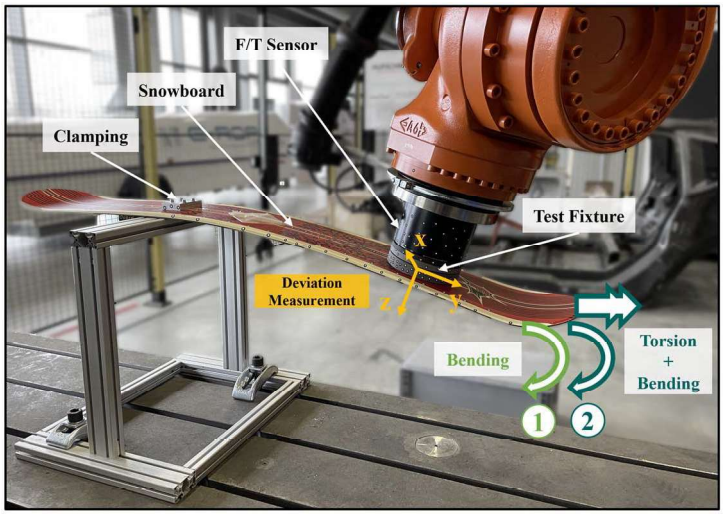

the *x*- and *y*-axis. The torque around *z* has been adjusted because this rotation mainly loads the screw connection and is not the desired direction for the application of force. The bending and torsion in load case #2 were applied via a fixed connection between the robot and the snowboard, but only the torque was used to control the robot test motion. For this case, the displacements of the different parts have been measured by optical tracking of the markers on the snowboard. The ATOS 5 was used as the optical measurement system with CP40/MV1000 lenses, which can examine a volume of 1, 000 × 750 × 750 mm^3 (calibration deviation: 0.027 pixels).

Results and Discussion

UNIAXIAL STRESS STATES WITHOUT TRANSVERSE FORCES

Results

Four stress–strain curves are plotted in figure 7 to compare the different testing conditions. Three curves display the results for the robot-based tensile tests, each corresponding to a control mode in the robot-based tests. Each single curve shows the averaged values over three tested specimens. One further curve represents the average value obtained from four specimens tested using the universal testing machine.

The curves of the robot-based force control, based on the raw data, showed high fluctuations in the stress–strain diagram due to the control. To achieve a significant value for the tensile strength, the robot-based force-controlled curve (gray) in figure 7 was smoothed (moving average, points of window: 50). Table 1 summarizes the material properties after evaluation. The Young's modulus (E), tensile strength (R_m), elongation at fracture (A_t), Poisson's ratio, and yield strength ($R_{p0.2}$) were evaluated. To determine the arithmetic mean and the standard deviation in Table 1, three repetitions or tensile specimens per control type were performed for the robot-based tensile tests and four for the classic tensile tests on the universal testing machine. The gage length corresponds to the parallel length of the dog-bone shaped tensile specimens of 80 mm. To determine engineering strain, a surface component was generated for each tensile specimen (DIC). This means that the resulting strain values are evaluated on the full area, and not solely points. The Young's modulus was determined for the individual measurements using a linear regression in the strain range 0.01 to 0.15 %. Smoothed curves were also used to evaluate the tensile strength R_m of the robot-based force-controlled tensile tests in Table 1.

To verify the accuracy of the compensation of transverse force by sensor-guided test motions, the position deviations (see fig. 8) and resulting transverse forces (see fig. 9) were examined in more detail. In contrast to

FIG. 7 Stress–strain diagram for tensile testing. Four test conditions are compared: force, path, and position control, according to the internal robot control, and position control on the universal testing machine. The three different control modes of the robot-based testing were based on three specimens each time. For the tensile testing in the laboratory, four specimens have been considered.

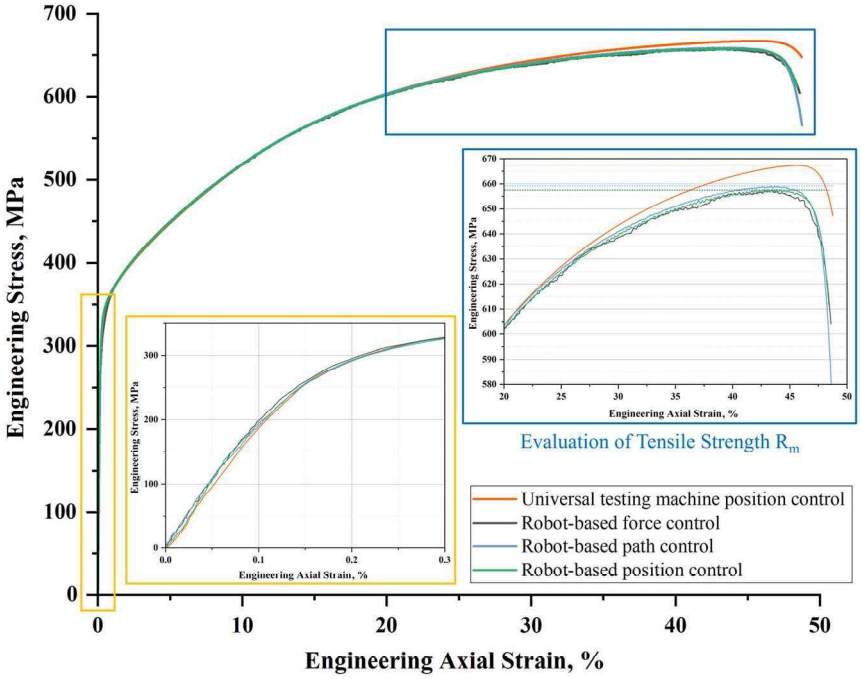

TABLE 1
Comparison of material properties of robot-based tests and the tests performed on the universal testing machine

Type of Test	Young's Modulus E, GPa	Tensile Strength R_m, MPa	Elongation at Fracture A_t, %	Poisson Ratio	Yield Strength $R_{p0.2}$, MPa
Robot-based force control	211.5 ± 4.3	656.3 ± 1.4	49.1 ± 0.5	0.29 ± 0.01	336.2 ± 1.4
Robot-based path control	202.6 ± 1.2	659.4 ± 1.3	48.8 ± 0.0	0.27 ± 0.02	334.7 ± 0.4
Robot-based position control	215.1 ± 3.2	657.8 ± 1.2	49.1 ± 0.5	0.29 ± 0.01	335.0 ± 0.5
Universal testing machine position control	201.0 ± 8.8	668.9 ± 7.0	53.1 ± 2.6	0.28 ± 0.01	336.0 ± 1.3

Hanke et al.,[13] in which force and path deviation data from robot-based measurements have already been published as preliminary studies based on only one specimen, the results published as part of this study are based on several specimens per test type. Each curve represents an average value over the tensile tests of the respective robot-based tests and the conventional tests. To evaluate the displacements in the x and y directions, two coordinate systems (see fig. 4) were placed in the center of the clamping jaws, and both the distances in the x-, y-, z-directions and the three associated rotation angles (six degrees of freedom [6DOF]) were measured in relation to each other using the optical measurement system. The stationary clamping jaw served as a reference. In the robot-based tests, the upper clamping jaw, which is connected to the industrial robot, is moved relative to the position of the stationary lower clamping jaw. In figure 8, the measured deviations in the x- and y-direction are depicted in blue for the path control mode. After a short settling, the deviation in the x- and y-direction approaches zero (fig. 8) because it is immediately corrected by the control loop. In comparison, the curve for the position control of the robot shows an increasing deviation as function of time (green line, fig. 8). No sensor-based control is used

FIG. 8 Averaged deviation of positions with standard deviation in x-direction (left picture *A*) and y-direction (right picture *B*) for the different robot-based tests and the tests performed on a universal testing machine.

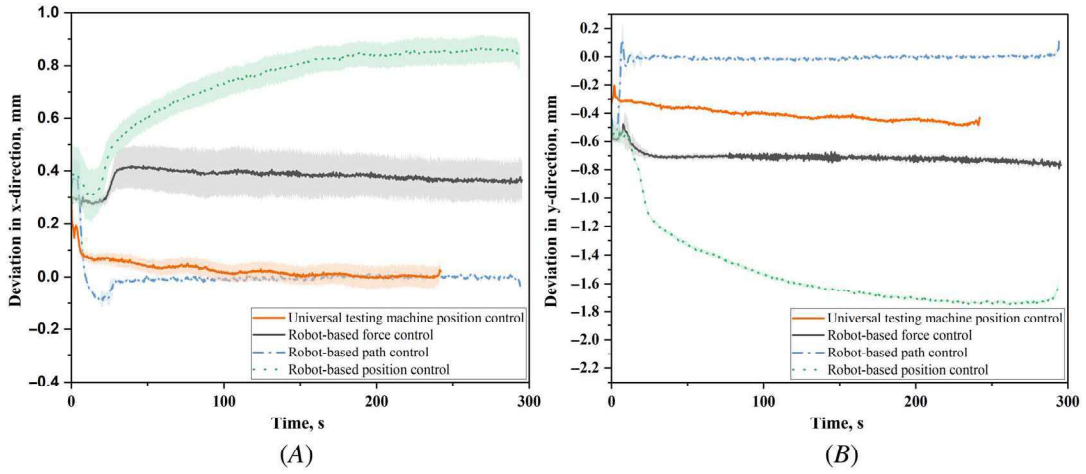

here, resulting in a deviation that is significantly higher compared with the other curves. The curve for force control (gray curve, fig. 8) settles at a constant value in both directions but results in a significant offset in both directions. For comparison, the results of the universal testing machine show a relatively high initial value of 0.2 mm in the *x*-direction. After the initial peak, the deviation decreases from 0.1 mm to almost zero. In the *y*-direction, the deviation starts at −0.25 mm and slowly increases to −0.5 mm. These deviations at the beginning of the test on the classic universal testing machine indicates that the center position of the upper and lower clamping jaw deviates slightly from an ideal line in the test laboratory. This initial deviation changes during the test once load is applied.

Figure 9 shows the transverse forces F_x and F_y as a function of the testing time only for the robot-based testing. Because our universal testing machine was not equipped with multiaxial load cells, we were not able to capture the transverse loads. In the curve for force control (gray line, fig. 9), the transverse forces are compensated below 5 N during the measurement. However, this corresponds to a systematic deviation in the position, as seen in figure 8.

FIG. 9 Averaged transverse forces F_x (left picture *A*) and F_y (right picture *B*) with standard deviation for the different robot-based tests.

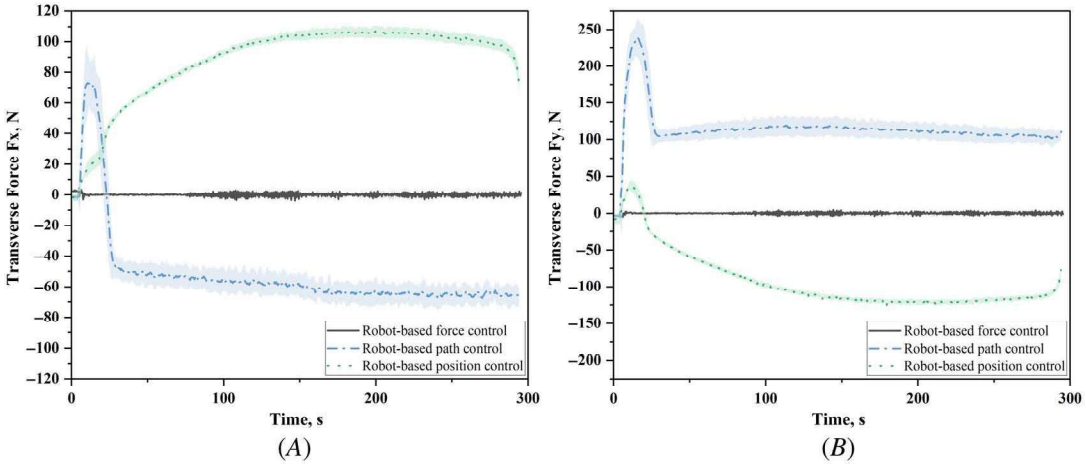

In contrast, the path control with the internal robot control (blue line, fig. 9) shows an initial settlement corresponding to the settlement of positions in figure 8 followed by a constant, yet high value of both components F_x and F_y. The position control mode (green line, fig. 9) consistently has the highest transverse forces (F_x over 100 N, F_y over 125 N), and thus neither realizes a pure uniaxial stress nor a pure uniaxial strain state.

Discussion

Within the margin of error of Table 1, there is only a slight difference between the results of the robot-based and conventional testing. Both test conditions, robot-based and conventional tensile testing, agree with the tensile strength, elongation at fracture, and yield strength from the material suppliers datasheet. The high Young's modulus of 211.5 GPa (robot-based force control) and 215.1 GPa (robot-based position control) is recognized. However, the primary objective is to ensure comparability between different setups and methods, rather than determining mechanical characteristics. During the tests, efforts were made to maintain consistency between the robot-based and conventional tensile testing setups. This involved using the same image correlation system (ATOS 5), identical lenses, and therefore the same measurement distance. The speckle pattern was applied using a consistent method and pattern coarseness to facilitate a meaningful comparison. Furthermore, the same pixel size (0.18 mm/pixels) and incision deviation (under 0.1) were used throughout all tensile tests. Additionally, the high standard deviation observed in the conventional test laboratory was investigated. It was found that among the four tested samples, one exhibited significantly high deviations in Young's modulus (216.1 GPa), tensile strength (656.9 MPa), and elongation at fracture (48.8 %). The other samples demonstrated much more consistent results. Consequently, the arithmetic mean and standard deviation were recalculated using only the three remaining samples, resulting in Young's modulus $E = 196.0 \pm 1.7$ GPa, tensile strength $R_{m=}672.9 \pm 1.2$ MPa, and elongation at fracture $A_t = 54.6 \pm 0.69$ %.

Based on the evaluation of displacements, the test condition of the universal testing machine is closest to the path control mode of the robot testing. For these two cases, the experimentally obtained values agree within the margin of error. In addition, the curve of the classical tests agrees very well with the robot-based tests in the linear elastic range of the stress–strain diagram (see fig. 7). Only when close to the ultimate strength does a slight deviation between the curves become visible. Because the universal testing machine is operating in path-controlled mode, there is a likely build-up of transverse forces similar to the robot-based test setup visualized in figure 9. Based on the measured offset in the x- and y-axis in figure 8, it can be assumed that the transverse forces are considerable, but not exactly known, because the load cell of the universal testing machine is only uniaxial. It is well-known that uniaxial load cells are strongly affected by superimposed transverse forces, therefore compromising the actual reading. Therefore, it can be assumed that the remaining discrepancy is an actual deficiency of the load cell in the universal testing machine and is not caused by the robot-based setup.

Figure 8 shows that the path control for a quasistatic uniaxial test motion could be implemented. All displacements transverse to the load direction can be successfully compensated. As a result, fewer transverse forces occur than without sensor control. The force control can be successfully implemented because all transverse forces can be compensated (see fig. 9). The deviations transverse to the load direction (in the x- and y-directions) can be significantly reduced compared with the position control by the internal robot control.

VARIATION OF LOAD VECTOR POSITION

Results

With the three load cases of the bicycle frame performed, it was possible to demonstrate that the position of the load vector on the component can be varied flexibly. This means that a complete load specification can be tested in one test setup. All three positions were successfully tested with path and force control. In the following, load case #2 (compression on the seat tube) is described in more detail as an example of the three defined load cases. In path control, the deviations transverse to the test direction (z-direction) between the center of the test fixture and the center of the bicycle seat tube are the controlled variable. For force control, these are the transverse forces F_x and F_y. All control variables are assigned the value 0.

FIG. 10 Bicycle frame test load case #2: the compression load of about 2,000 N on the seat tube with the help of the path control (left picture *A*) or with the force control (right picture *B*).

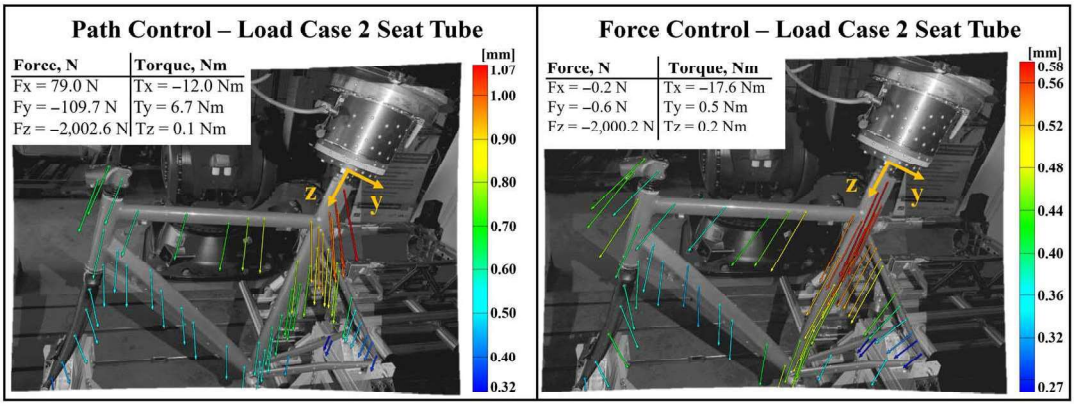

(*A*) (*B*)

Figure 10 shows the end of the test at the maximum load of F_z at approximately −2,000 N. The images are taken by the optical measurement system. The measured displacements of the bicycle frame are shown as arrows pinned at the respective optical markers. The maximum displacement (red arrows) takes place close to the location of force application. This is 1.07 mm in figure 10*A* (path control) and 0.58 mm in figure 10*B* (force control) at effectively the same load. The direction of the arrow indicates the direction of the displacement; the color code represents the magnitude. The different displacements are due to the different local orientations of the resulting deformation. In force control (see fig. 10*B*), the load can be directed along the axis of the seat tube. This type of force application results in a deformation that is directed differently and causes less maximum displacement. Because of the bicycle frame geometry, greater stiffness is expected when the force is applied in the direction of the seat tube axis (so in the case of force control) than when the force is a response to a deformation in path control.

In addition, the forces and torques at the end of the test are also shown in figure 10. In the force-vector controlled test (fig. 10*B*), the transverse forces are compensated and are converging to 0 N. Torques are only present in the *x*-direction with −17.6 Nm.

Discussion

The testing of the bicycle frame highlights that robot-based testing is also possible for more complex stiff geometries at the component level. Likewise, sensor-guided motions could successfully be implemented to realize three different load cases. Here, the path-controlled approach leads to special challenges. Because of the complex geometries of the test fixtures and the bicycle frame, it is much more challenging to define an appropriate coordinate system. Thus, a new method is required to define the coordinate system in the component and in the test fixture to enable a path-controlled motion. Therefore, the existing STL files are imported into the measurement software for the optical measurement. In this environment, the required points for path control can be determined, such as the point of application of force on the bicycle frame or the center of the test fixture. A coordinate system is placed in each of these points. Overall, across all three load cases, it can be observed that the path-controlled tests are more complex and less accurate to implement than the force-controlled tests because of the challenge in defining an adequate path. Depending on the test fixture, there was a deviation of approximately 1 mm between the position determined in the measurement software and the actual position of the center points of the bicycle frame and test fixture (transmission point for the force) in the path-controlled tests. This could be determined on the basis of the precisely modeled form-closured test fixtures. The lack of compensation between different coordinate systems

may be one reason for the high transversal forces in the path-controlled test, as shown in figure 10. These have much higher values compared with the path-controlled tensile tests (blue curve fig. 9), indicating that the generation of a three-dimensional motion is more challenging to exclude. Therefore, force control is found more suitable for testing of complex geometries because it allows for directly controlling the applied load vector.

SUPERPOSITION OF LOAD CASES

Results

This subsection presents the results of the pure bending tests (load case #1, fig. 6) and the snowboard's superimposed bending and torsion test (load case #2, fig. 6). As mentioned, the snowboard is characterized by its high compliance. Thus, the snowboard behaves differently than the much stiffer bicycle frame and the tensile test specimens. The requirements for the control system rise with increasing compliance of the component because of the greater travel distances of the industrial robots (depending on the test speed). This results in higher requirements for the latency and response time of the control system. The results of pure bending (load case #1) for path and torque control are summarized in figure 11. The force, torque, deviation, and angle of rotation in all three spatial directions are shown over time. The torques are the control variables for torque control, and the three angles of rotation and the deviation in the x- and y- directions are for path control. In both cases, it can be shown that the control has been successfully implemented. Similar to the tensile tests, the deviations in figure 11 were evaluated between two coordinate systems in the GOM Correlate software using 6DOF (in the x-, y-, z-directions and the corresponding rotation angles). One coordinate system was placed in the adapter plate on the snowboard side and another coordinate system was placed in the adapter plate on the robot end effector side. Both coordinate systems are almost in the same position, so only one is shown in figure 6 for clarity.

The capability of the system to adapt the load vector is illustrated in the pure bending test. The rotation angles between the snowboard and the robot end effector, shown in figure 11, are close to 0° during path control and can maintain this value constantly during the test. This means that the load vector is at the same perpendicular angle to the snowboard at the end as at the start of the test. The rotation angles for torque control show a slight change (maximum 0.2°) during the test. Nevertheless, it can be shown that the load vector can also be adapted to the deformation of the snowboard in real-time during torque control within this level of accuracy.

In the torque control of the pure bending test, a fixed connection was created between the test fixture and the snowboard. Because of the tension caused by this fixed connection, the initial value of the forces and torques is significantly higher than in the path control. The torques can be successfully reduced during the test and are lower than the torques occurring during path control. Because of the unpredictable mutual influences of the forces and torques, we were unable to implement simultaneous torsional and force control. For this reason, the decreasing force F_x of approximately 100 N toward the end of the test is a sufficient result for the moment.

The results of the superimposed bending and torsion test are shown in figure 12. In figure 12*A*, the displacement of the snowboard at the highest force and torque level is depicted. The deviation was determined between the global (fixed) coordinate system placed in the clamp of the snowboard and the local (movable) coordinate system in the adapter plate connecting the force/torque sensor at the end effector of the robot and the snowboard (see fig. 12). As expected, the displacement is highest at the free end of the snowboard, with 98.62 mm in total. The values of forces and torques at the end of the test are shown in figure 12. Because the forces and torques influence each other, it is not possible to simultaneously rule out the torques and the forces in our experimental setup. Figure 12*B* shows all three torque curves. The continuous increase of the torque T_y is visible and intended by the test definition. The torques T_x and T_z are compensated by the control. Figure 12*C* shows the axial force curve for all three spatial directions. Here, F_y increases continuously because of the influence of the torques. Considering the bending, F_z also decreases constantly.

The forces F_x and F_y start with an offset of approximately 200 N offset because of residual forces that occur during the clamping process. The initial values of the torques T_x and T_y also originate from the fixed clamping of the snowboard.

FIG. 11 Four graphs (force, torsion, displacement, angle of rotation over time) each for torque control and path control.

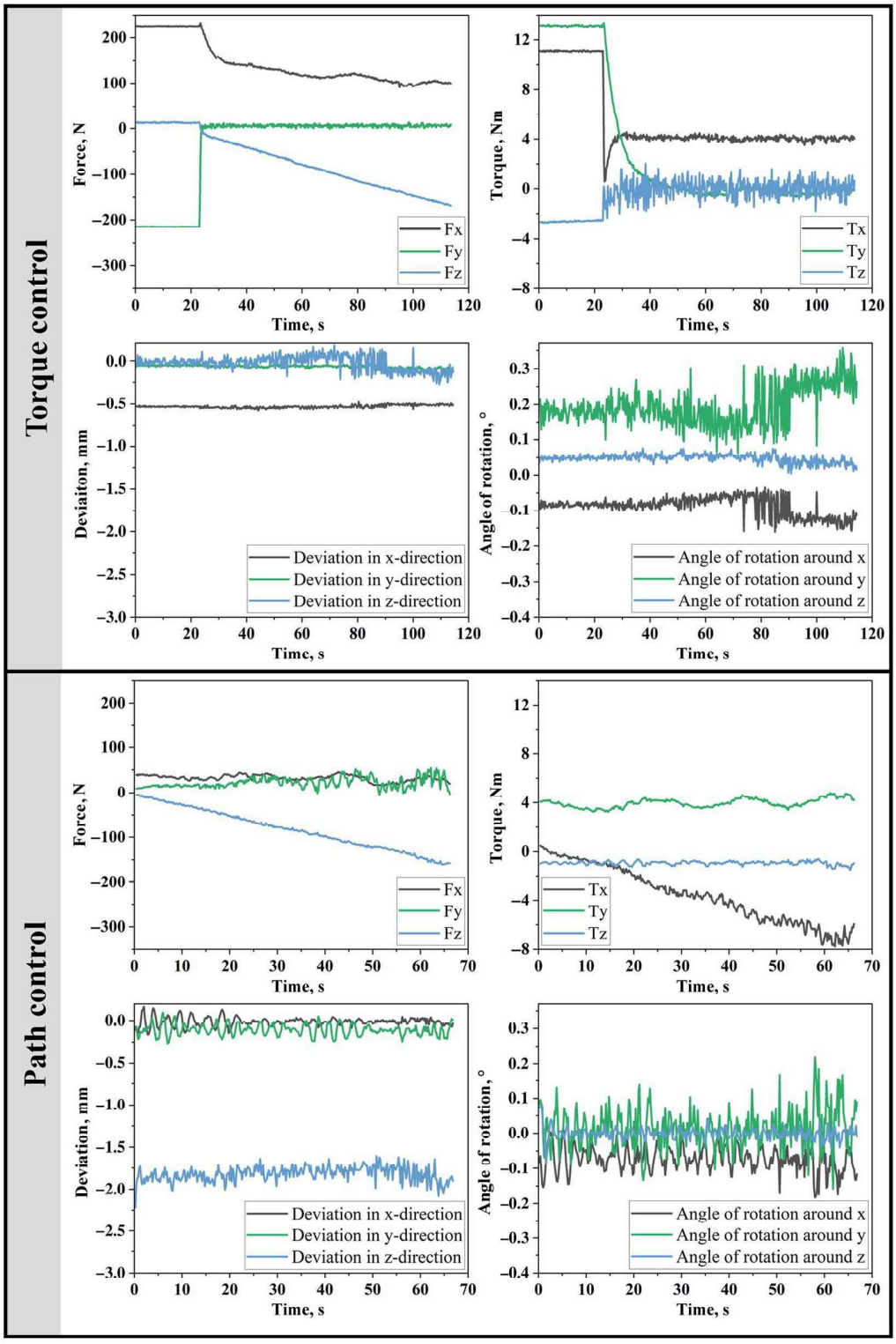

FIG. 12 Superimposed loads of bending and torsion in snowboard testing: (*A*) The absolute displacement of the snowboard and the force/torque at the end of the test, (*B*) the force, and (*C*) torque curves.

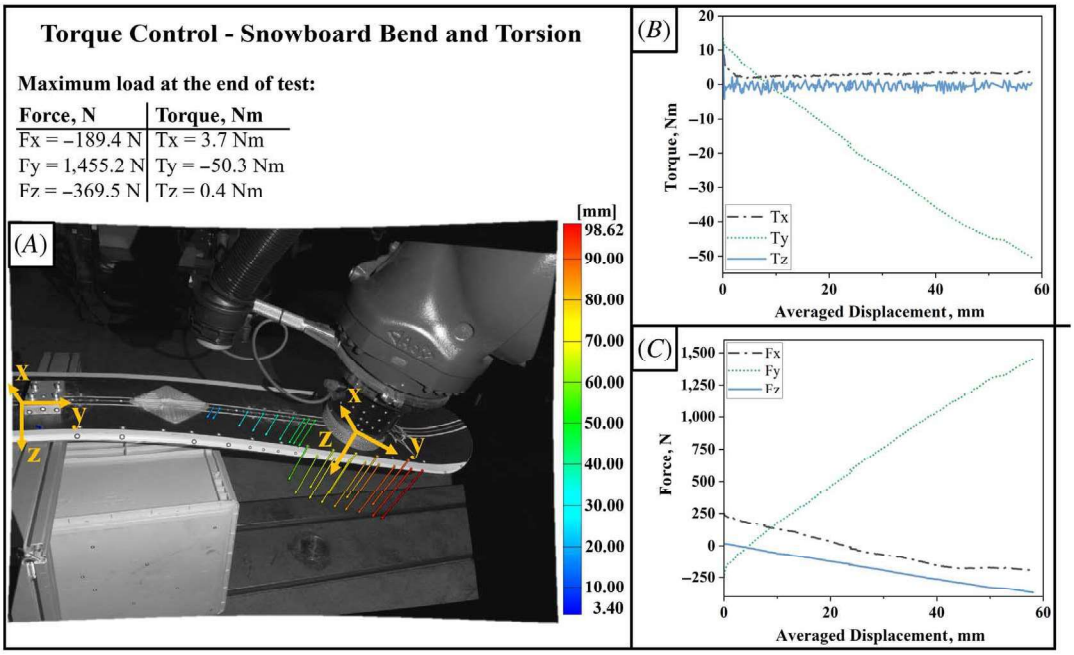

Discussion

Complex 2-D testing motions in terms of bending as well as superimposed bending and torsion were realized with the described test setup of the snowboard. A fixed connection between the two test fixtures is not necessary for the path-controlled bending test setup. This means that a displacement of the upper test fixture relative to the lower one is immediately visible and measurable. In contrast to the bicycle frame tests, the cylindrical test fixture on the snowboard and on the end effector of the industrial robot were precisely measured using a tactile measuring method. This means that the precision of the path control depends on the complexity of the geometry of the test fixture and the component. Similar to the tensile tests, constant small deviations also occur here (torque control: −0.5 mm in *x*-direction, path control: −2.0 mm in *z*-direction). The coordinate systems were not at the same height at the beginning of the test because the snowboard already shows bending at the beginning because of its own weight with this type of mounting. Additionally, in the torque-controlled snowboard test, the adapter plates between the robot end effector and the snowboard were firmly connected. In the path-controlled test, however, the plates are only loosely placed on top of each other. Therefore, the distance between the adapter plates (and thus the deviation in the *z*-direction) is slightly greater in the path control test. Despite this, no relevant deviation could be detected (see fig. 11). Similarly, no change in the angle of rotation could be detected during the test (see fig. 11). The load vector can therefore be tracked very precisely during the deformation of the snowboard. This shows that the robot-based test meets the real-time requirements of a component test and that the control loop works conveniently despite the high flexibility and compliance of the component.

The desired superimposed load from bending and torsion can be successfully realized using the snowboard test. Torque control can be used to apply a defined superimposed load to a flexible component. These tests are only intended to serve as an example and demonstrate that the approach can also be transferred to other superimposed load cases.

Conclusions

The aim of this study is to demonstrate the feasibility of robotic-based mechanical testing from classical laboratory sized specimens up to complex components. This was successfully demonstrated using tensile tests as a typical materials characterization task and a bicycle frame and a snowboard as representative components.

These specimen tests were used to demonstrate the flexibility of robot-based testing regarding the geometry of the test object as well as the type of load and control mode. With the possible 6DOF, industrial robots can perform every conceivable test motion. This means that various complex and superimposed test motions can be performed. Another advantage is that the load vector can be moved along with the deformation of the component during a sensor-guided motion. This means that the force application point and the orthogonal angle of the force vector between the component and the force vector remain unchanged during the test.

The influence of the different control modes (path control, force control, and position control) was evaluated in the context of uniaxial loading of tensile test specimens and found in reasonable accordance with classical tests. Robot-based component testing has been used to successfully inspect more complex geometries using path and force-controlled configurations. For highly compliant components, it was demonstrated that a continuous adjustment of the load vector is possible. In addition, the possibility to use superimposed loads was demonstrated for a combination of bending and torque.

ACKNOWLEDGMENTS

This work has been developed in the BMBF-funded project "WiR–Wissenstransfer Region Augsburg" (reference number: 3IHS040) at the University of Augsburg. The authors thank Stefan Wolff and Stefan Schmitt for their support and help in realizing the experimental setups.

References

1. R. Damaševičius, R. Maskeliunas, G. Narvydas, R. Narbutaitė, D. Połap, and M. Woźniak, "Intelligent Automation of Dental Material Analysis Using a Robotic Arm with Jerk Optimized Trajectory," *Journal of Ambient Intelligence and Humanized Computing* 11, no. 12 (December 2020): 6223–6234, https://doi.org/10.1007/s12652-020-02605-8
2. P. B. Khoi, H. T. Hai, and T. M. Thuy, "An Error Compensation Controller for Milling Robots," *Vietnam Journal of Mechanics* 45, no. 2 (June 2023): 105–116, https://doi.org/10.15625/0866-7136/16979
3. C. Ji, J. K. Na, Y.-S. Lee, Y.-D. Park, and M. Kimchi, "Robot-Assisted Non-destructive Testing of Automotive Resistance Spot Welds," *Welding in the World* 65, no. 1 (January 2021): 119–126, https://doi.org/10.1007/s40194-020-01002-1
4. P. Wang, X. Dong, Y. Yang, and Y. Cheng, "Robot-Assisted Trajectory Planning Method for NDT," in *2023 IEEE Sixth International Conference on Industrial Cyber-Physical Systems (ICPS)* (Piscataway, NJ: IEEE, 2023), 1–6, https://doi.org/10.1109/ICPS58381.2023.10128074
5. M. Gupta, M. A. Khan, R. Butola, and R. M. Singari, "Advances in Applications of Non-destructive Testing (NDT): A Review," *Advances in Materials and Processing Technologies* 8, no. 2 (April 2021): 2286–2307, https://doi.org/10.1080/2374068X.2021.1909332
6. C. Mineo and Y. Javadi, "Robotic Non-destructive Testing," *Sensors* 22, no. 19 (October 2022): 7654, https://doi.org/10.3390/s22197654
7. F. Beeh and H. Wörn, "Occubot VI - An Intelligent Robot System for Seat Testing Applications," in *Intelligent Autonomous Systems* 7, ed. M. Gini, W. M. Shen, C. Torras, and H. Yuasa (Amsterdam, the Netherlands: IOS Press, 2002), 26–29.
8. M. Nierenberger, M. Poncelet, S. Pattofatto, A. Hamouche, B. Raka, and J. M. Virely, "Multiaxial Testing of Materials Using a Stewart Platform: Case Study of the Nooru-Mohamed Test," *Experimental Techniques* 38, no. 2 (March/April 2014): 74–83, https://doi.org/10.1111/j.1747-1567.2012.00807.x
9. K. Alemzadeh and D. Raabe, "Prototyping Artificial Jaws for the Bristol Dento-Munch Robo-Simulator; 'A Parallel Robot to Test Dental Components And Materials'," *in 2007 29th Annual International Conference of the IEEE Engineering in Medicine and Biology Society* (Piscataway, NJ: IEEE, 2007), 1453–1456, https://doi.org/10.1109/IEMBS.2007.4352574
10. M. Kebbach, R. Grawe, A. Geier, E. Winter, P. Bergschmidt, D. Kluess, D. D'Lima, C. Woernle, and R. Bader, "Effect of Surgical Parameters on the Biomechanical Behaviour of Bicondylar Total Knee Endoprostheses - A Robot-Assisted Test Method Based on a Musculoskeletal Model," *Scientific Reports* 9, no. 1 (October 2019): 14504, https://doi.org/10.1038/s41598-019-50399-3

11. J. Hanke, C. Eymüller, J. Reichmann, A. Trauth, M. Sause, and W. Reif, "Software-Defined Testing Facility for Component Testing with Industrial Robots," *in 2022 IEEE 27th International Conference on Emerging Technologies and Factory Automation (ETFA)* (Piscataway, NJ: IEEE, 2022), 1–8, https://doi.org/10.1109/ETFA52439.2022.9921625
12. J. Hanke, "Robot-Based Component Testing on Software-Defined Test Benches" (PhD diss., Universität Augsburg, 2024).
13. J. Hanke, C. Eymüller, A. Poeppel, J. Reichmann, A. Trauth, M. Sause, and W. Reif, "Sensor-Guided Motions for Robot-Based Component Testing," in *2022 Sixth IEEE International Conference on Robotic Computing (IRC)* (Piscataway, NJ: IEEE, 2022), 81–84, https://doi.org/10.1109/irc55401.2022.00021
14. J. Hanke, M. Stueben, C. Eymüller, M. Müller, A. Poeppel, and W. Reif, "CASP: Computer Aided Specimen Placement for Robot-Based Component Testing," in *Proceedings of the 20th International Conference on Informatics in Control, Automation and Robotics 1: ICINCO* (Setúbal, Portugal: Scitepress, 2023), 374–382, https://doi.org/10.5220/0012155000003543
15. E. M. C. Jones and M. A. Iadicola, *A Good Practices Guide for Digital Image Correlation* (Clermont-Ferrand, France: International Digital Image Correlation Society, 2017), https://doi.org/10.32720/idics/gpg.ed1